Published in final edited form as:

Stem Cell Res. 2018 December ; 33: 100–109. doi:10.1016/j.scr.2018.10.015.

Derivation and characterization of putative craniofacial mesenchymal progenitor cells from human induced pluripotent stem cells

Mohamed Jamal[a,1], **Sara L. Lewandowski**[a], **Matthew L. Lawton**[a], **George T.-J. Huang**[c], **Laertis Ikonomou**[a,b,*]

[a]Center for Regenerative Medicine, Boston University and Boston Medical Center, Boston, MA, USA

[b]Pulmonary Center, Boston University School of Medicine, Boston, MA, USA

[c]Department of Bioscience Research, College of Dentistry, University of Tennessee Health Science Center, Memphis, TN, USA

Abstract

The introduction and widespread adoption of induced pluripotent stem cell (iPSC) technology has opened new avenues for craniofacial regenerative medicine. Neural crest cells (NCCs) are the precursor population to many craniofacial structures, including dental and periodontal structures, and iPSC-derived NCCs may, in the near future, offer an unlimited supply of patient-specific cells for craniofacial repair interventions.

Here, we used an established protocol involving simultaneous Wnt signaling activation and TGF-β signaling inhibition to differentiate three human iPSC lines to cranial NCCs. We then derived a mesenchymal progenitor cell (NCC-MPCs) population with chondrogenic and osteogenic potential from cranial NCCs and investigated their similarity to widely studied human postnatal dental or periodontal stem/progenitor cells. NCC-MPCs were quite distinct from both their precursor cells (NCCs) and bone-marrow mesenchymal stromal cells, a stromal population of mesodermal origin. Despite their similarity with dental stem/progenitor cells, NCC-MPCs were clearly differentiated by a core set of 43 genes, including ACKR3 (CXCR7), whose expression (both at transcript and protein level) appear to be specific to NCC-MPCs.

Altogether, our data demonstrate the feasibility of craniofacial mesenchymal progenitor derivation from human iPSCs through a neural crest-intermediate and set the foundation for future studies regarding their full differentiation repertoire and their *in vivo* existence.

*Corresponding author at: Center for Regenerative Medicine of Boston University and Boston Medical Center, 670 Albany Street, Room 211, Boston, MA 02118, USA. laertis@bu.edu (L. Ikonomou).

[1]Current address: Endodontic Department, Hamdan Bin Mohammed College of Dental Medicine, Mohammed Bin Rashid University of Medicine and Health Sciences, Dubai, United Arab Emirates.

Conflicts of interest

The authors declare that they do not have any conflicts of interest.

1. Introduction

Neural crest (NC), a multipotent, transient structure during vertebrate development, is the precursor to a wide variety of cell types, such as mesenchymal, pigment, neuronal, and glial cells in various tissues (Dupin and Le Douarin, 2014). This is due to the formidable migratory capacity of NC cells (NCCs) along defined trajectories following an epithelial-to-mesenchymal transition and to their ability to give rise to specialized subpopulations with specific differentiation repertoires (cranial, vagal, trunk, and cardiac NCCs).

Most information on NC development comes from studies in *in vivo* avian and murine systems (Dupin and Le Douarin, 2014). The use of human *in vitro* NCC-based systems would undoubtedly be a powerful tool in the elucidation of basic questions at a stage of human development that is essentially inaccessible *in vivo*. Additionally, *in vitro* derivation of human cranial NCCs is a prime target in craniofacial and dental tissue engineering, as cranial NCC derivatives include osteocytes, chondrocytes, and dental cells, such as odontoblasts, pulp, and periodontal ligament cells (Chai et al., 2000). Human pluripotent stem cells (PSCs) offer such a system and the advent of induced pluripotent stem cells (iPSCs) has opened up the exciting possibility of tailored NCCs derived from individuals with pathologies related to NC development. Indeed, considerable progress has been made towards the derivation of NCCs from human PSCs, including human iPSCs (hiPSCs), by manipulation of signaling pathways involved in NC specification (Chambers et al., 2009; Huang et al., 2016; Jiang et al., 2009; Menendez et al., 2011; Mica et al., 2013). For example, Dalton and coworkers have demonstrated that inhibition of SMAD signaling in concert with WNT signaling activation (through GSK-3β inhibition) results in the establishment of a highly enriched NCC population from human PSCs (Menendez et al., 2013; Menendez et al., 2011). Moreover, Weiss and co-workers identified retinoic acid (RA) as a critical signal for the derivation of specific NCC subtypes, namely cranial (absence of RA) and trunk (presence of RA) (Huang et al., 2016).

Here, we investigate the possibility of deriving mesenchymal progenitors through a NC intermediate from hiPSCs. To this end, we derived and extensively characterized NCCs from hiPSCs. We subsequently differentiated NCCs to mesenchymal progenitors with robust osteogenic and chondrogenic differentiation potential and performed genome-wide microarray analysis of these two populations along with known human dental stem/progenitor cell populations such as dental pulp stem cells (DPSCs) (Gronthos et al., 2000), stem cells of the apical papilla (SCAP) (Sonoyama et al., 2008), periodontal ligament stem cells (PDLSCs) (Seo et al., 2004), and bone marrow derived mesenchymal stromal cells (BMSCs), a mesenchymal population of mesodermal origin. NCC-derived progenitors were characterized by a high degree of similarity to dental stem/progenitor cell populations and were clearly distinct from both NCCs and BMSCs. At the same time, several unique markers of these progenitors were identified, including cell surface molecules, such as *CXCR7* and *PTPRB*, and transcriptional regulators, such as *MEIS2* and *ANKRD1*.

2. Results

2.1. Derivation and characterization of putative neural crest cells from human pluripotent stem cells

We hypothesized that derivation of bona fide craniofacial mesenchymal progenitors from human pluripotent stem cells should take place through a cranial (cephalic) neural crest intermediate. To this end, we first used an established protocol to derive and characterize neural crest cells (NCCs) (Menendez et al., 2013). In the original protocol, simultaneous and sustained activation of Wnt signaling by (2′Z,3′E)-6-bromoindirubin-3′-oxime (BIO) (a GSK-3β inhibitor) and inhibition of transforming growth factor β (TGF-β) signaling by SB431542 was used to derive highly enriched NCC cultures. In our modified protocol, we substituted a more selective GSK-3β inhibitor (CHIR) for BIO (Ring et al., 2003). In brief, BU3-hiPSCs were cultured in media containing CHIR to activate Wnt signaling and SB431542 to inhibit TGF-β signaling (NCC media). The population of cells co-expressing HNK1 (B3GAT1, also known as CD57) and p75 (NGFR, also known as CD271) was monitored by flow cytometry (Fig. 1B). Cells with lower p75 levels were eliminated by repeated passaging in NCC media and by Day(D) 35–40 we observed the derivation of putative NCCs, characterized by spindle-like morphology, co-expression of high HNK1/p75 levels (Fig. 1A,B and Fig. S2B) and gene expression of the EMT-related transcription factors, *SNAI1* and *SNAI2 (SLUG)* (Fig. S2C). High and uniform SNAI1 expression was also confirmed by immunocytochemistry (Fig. S2C). We were able to reproducibly derive this population from three hiPSCs lines (Figs. 1B, S1A and S2A).

To further understand the identity of the derived cells, we characterized the expression kinetics of known NCC markers (Simoes-Costa and Bronner, 2015) at various time points of NCC derivation (Fig. 1C). More specifically, we looked at representative genes from the neural plate border module (*PAX3*, *ZIC1*), and the neural crest specification/migration modules (*PAX3, SOX9, SOX10, FOXD3, ETS1*).

The neural plate border specifier *PAX3* was continuously expressed since D5 with a slight decrease in expression by D34 (Fig. 1C and S1B) whereas *ZIC1* was only expressed after D25. Genes, such as *SOX9* and *ETS1*, that mark neural crest specified cells, were continuously expressed from D5 on and reached their highest expression levels at later time points (D25-D34) and this pattern of expression coincided with establishment of a homogeneous cell population, as shown by flow cytometry (Figs. 1B,C). Interestingly, two other neural crest specifier genes, *SOX10* and *FOXD3*, were continuously expressed during NCC differentiation of hiPSCs but their expression was downregulated in the final population. Importantly, expression of *PAX6*, a neural progenitor marker, was low throughout NCC differentiation and completely abrogated by D34 (Fig. 1C).

We then tried to understand the potential functional significance of the two populations with differential p75 expression, observed during NCC derivation by sorting these populations on D15 and performing RT-qPCR analysis (Fig. 1D). Neural plate or neural crest specifiers were found to have either similar expression levels in the two populations or higher expression levels in the $p75^{bright}$ population (Fig. 1D and S2D). Of note, *ETS1*, a key cranial neural crest marker was enriched in the $p75^{bright}$ population (Fig. 1D and S2D).

On the contrary, *PAX6* and *PHOX2B*, a neuronal and trunk NCC marker respectively (Huang et al., 2016), were enriched in the $p75^{dim}$ population and were not expressed in the D37-D45 $p75^{bright}$ population. This suggests that neuronal and trunk NCC "contaminants" were eliminated during cranial NCC differentiation, probably through the combined means of soluble factor signaling and repeated cell passaging.

Overall, the above data indicate that sustained WNT signaling activation and TGF-β inhibition lead to the robust and reproducible derivation of a cell population with cranial NCC characteristics from several hiPSC lines. This further supports the general applicability of the protocol introduced by Dalton and colleagues (Menendez et al., 2013).

2.2. Cranial NCCs can give rise to mesenchymal progenitor cells

We then proceeded to derive mesenchymal progenitor cells (MPCs) from our NCC population using culture media with high FBS content (10%) (Fig. 2A). Several cell surface markers of the resulting putative MPCs were characterized by flow cytometry and their competence to undergo tri-lineage (chondrogenic, osteogenic and adipogenic) differentiation was also evaluated (Figs. 2B,D and S1C) (Dominici et al., 2006). As shown in Figs. 2B and S1C, putative mesenchymal progenitor cells (NCC-MPCs) derived from three hiPSC lines exhibited the same cell surface marker profile with all populations being almost 100% positive for CD73, CD90, CD105 and CD146. On the contrary, these cells were negative for hematopoietic (CD45), monocyte (CD14) and NCC markers (HNK1 and p75), with the latter finding strongly suggesting efficient conversion of human NCCs to NCC-MPCs under high FBS culture conditions. Additionally, all three NCC-MPC lines showed very similar morphologies during expansion (Fig. 2C) and expressed mesenchymal cell-like markers such as ACTA2 and VIM (Fig. S4A). Two of the three lines (BU3 and BU7) exhibit robust osteogenic and chondrogenic differentiation in respective media whereas BU1 iPSC differentiation to the same cell types was less efficient (Fig. 2D), probably reflecting the inherent variability in differentiation potential of hiPSC lines (Osafune et al., 2008). Interestingly, the adipogenic differentiation protocol resulted in an immature adipocyte phenotype for all three lines (Fig. 2D, middle panels).

Taken together, these data demonstrate the efficient derivation of putative NCC-MPCs with osteogenic and chondrogenic, and to a lesser extent, adipogenic potential from human NCCs.

2.3. Genome-wide transcriptomic analysis of hiPSC-derived NCCs and NCC-MPCs

To gain further insights into the genetic programs of both the NCCs and their NCC-MPC progeny, we performed genome-wide microarray analysis of these populations along with known human dental stem/progenitor cell populations such as DPSCs (Gronthos et al., 2000), SCAP (Sonoyama et al., 2008) and PDLSCs (Seo et al., 2004) and bone marrow derived MSCs (BMSCs). As shown in the principal component analysis (PCA) plot (Fig. 3A), NCCs clearly separated from both dental and bone marrow stromal cell populations along the PC1 axis (29% of experimental variation). Additionally, the NCC-MPCs clustered roughly together with the dental stem/progenitor cell populations, and the BMSCs separated from both the NCCs and all mesenchymal-like cell populations along the PC2 axis (11%

of experimental variance). Taken together, this indicates that NCCs and mesenchymal-like stem/progenitor cells were quite different, whereas non-bone-marrow-derived mesenchymal-like progenitors were rather similar.

We then looked at gene expression differences to gain further insights in the biology of both NCCs and NCC-MPCs. When compared to BMSCs, NCC-MPCs had overall lower expression of *HOX* genes, reflecting a known *in vivo* difference between neural crest-derived and mesoderm-derived mesenchymal progenitor cells (Creuzet et al., 2002; Leucht et al., 2008) (Fig. S4B). A set of 1327 genes that were differentially expressed across groups (one-way ANOVA FDR $q < 10^{-6}$, |fold change| > 4 for any pairwise comparison between groups) were divided into 10 clusters (Fig. 3B). We focused on subsequent analysis on Cluster 1, which contains 482 genes that are strongly expressed only in NCCs. Within this cluster, there was strong expression of established NCC specifiers such as *SOX5/8/9*, recently identified transcriptional regulators of human NCC identity (*NR2F1* and *NR2F2*) (Rada-Iglesias et al., 2012; Rada-Iglesias et al., 2013), and transcription factors expressed in post-migratory NCC derivatives (*ALX3/4*) (Beverdam et al., 2001) (Fig. 3C). The uniformly high expression of a key cranial NCC marker, TFAP2A (de Croze et al., 2011; Menendez et al., 2013), was further confirmed by immunostaining (Fig. 3D). Surprisingly, Ingenuity Pathway Analysis revealed that most of the top pathways within Cluster 1 ($p < .001$) were related to cholesterol metabolism (Fig. 3E). Additional analysis of genes related to diseases and biological functions showed that genes contained in this cluster are associated with abnormal morphology of craniofacial structures such as maxilla, mandible, jaw bone, nasal septum and nose (Fig. S3A). Interestingly, genes that are part of these disease categories included *ALX4, CDON, ROR2, TCOF1, TFAP2A*, and *BMP7* (Fig. S3B) whose enhancers are bound by the nuclear receptors NR2F1/2 (Rada-Iglesias et al., 2012) that have highly enriched expression in our NCC population (Fig. 3C).

In summary, this analysis demonstrates that hiPSC-derived NCCMPCs are quite similar to known dental stem/progenitor cell populations. Furthermore, it further strengthens our RT-qPCR and cell surface analysis of hiPSC-derived NCCs and establishes the latter as a population distinct from bone marrow and dental mesenchymal progenitors.

2.4. NCC-derived NCC-MPCs are characterized by a unique transcriptional profile

To better understand the transcriptional profile of NCC-MPCs, we repeated our microarray analysis after excluding the BMSCs. The PCA plot showed, once again, clear separation of NCCs and mesenchymal progenitors along the PC1 axis (Fig. 4A). Nevertheless, NCC-MPCs were now clearly separated from all dental stem/progenitor cell populations, which appeared to greatly overlap (Figs. 4A and S4C). Of 1057 genes that were differentially expressed across groups (one-way ANOVA FDR $q < 10^{-5}$, |fold change| > 4 for any pairwise comparison between groups), a cluster of 43 genes (highlighted by a box in Fig. S4C) differentiated NCC-MPCs from dental stem/progenitor cells and NCCs. These genes included desmosomal-related genes (*DSC2/3*), transcription factors and nuclear receptors (*MEIS2*, *ANKRD1, SHISA2, NR2F2*), and cell surface molecules (*L1CAM*, *PTPRB*, *CXCR7* (*ACKR3*), *GPR126*). We validated five of these genes by RT-qPCR (highlighted in yellow in Fig. 4B). As shown in Fig. 4C, all five genes had significantly higher expression

in NCC-MPCs compared to dental stem/progenitor cells, with two of them (*PTPRB* and *ANKRD1*) also significantly more highly expressed in NCC-MPCs compared to NCCs.

Immunostaining of NCC-MPCs revealed almost ubiquitous expression of NR2F2 in all three lines examined (Figs. 5A,B and S5B), with a subset of these progenitors being also positive for MEIS2 (Fig. 5A). Most importantly, all three lines had high expression of the chemokine receptor CXCR7 (ACKR3) (Figs. 5C and S5A) whereas this receptor was not expressed in SCAP (Fig. 5D). Omission of primary antibodies resulted in complete absence of signal (Fig. S5C,D). We were not able to detect by immunohistochemistry any of the five validated NCC-MPC markers on paraffin sections of adult human dental pulp tissue (data not shown), which further corroborates their NCC-MPC specificity.

Taken collectively, the above data demonstrate that despite their similarity with known dental stem/progenitor cells, NCC-MPCs express, at the protein level, a distinctive combination of transcription factors and receptors. The functional implications of this finding are presently unclear and, as it is discussed below, warrant further studies of the NCC-MPC differentiation competence.

3. Discussion

Human cranial NCCs and their progeny are of particular interest to craniofacial research and tissue engineering. For instance, expanded autologous nasal chondrocytes have already been used to repairarticular cartilage defects in human subjects (Mumme et al., 2016). Additionally, an inexhaustible supply of cranial NCCs with broad differentiation potential is highly desirable. Human PSCs offer both an ideal model system to study fundamental questions in NC development and an advanced technological platform to derive clinically-relevant NCC derivatives, such as craniofacial osteoprogenitors and dental mesenchymal-like stem cells (Sharpe, 2016). In fact, features of neurocristopathies such as familial dysautonomia, and Hermansky-Pudlak and Chediak-Higashi syndromes have already been recapitulated *in vitro* using patient-specific iPSCs directed to a neural crest fate prior to disease-related cell derivation (melanocytes, peripheral neurons) (Lee et al., 2009; Mica et al., 2013). In the present work, we used a hiPSC-based system to a) define the global transcriptome of *in vitro* derived NCCs and b) derive putative craniofacial mesenchymal progenitors and study their relationship with known postnatal dental stem/progenitor cell populations.

First, we derived and extensively characterized putative NCCs from three hiPSC lines using a published directed differentiation protocol (Menendez et al., 2013). In our studies, the substitution of CHIR, a more specific GSK-3β inhibitor, for BIO did not appear to alter the identity of the end cell population derived after repeated passaging in the NCC differentiation media, as it will be discussed below. The successful derivation of bona fide cranial NCCs is supported by several lines of evidence. Genes with important regulatory roles in migratory cranial NCCs (*SOX9*, *ETS1*, *PAX3*) (Simoes-Costa and Bronner, 2015; Simoes-Costa et al., 2014) were upregulated in the NCC population whereas *PAX6*, a neuronal marker, and *PHOX2B*, a trunk NCC marker, were down-regulated. Our microarray analysis revealed an NCC-specific transcriptional signature (482-gene cluster)

that differentiated NCCs from all other cell populations (putative craniofacial, dental and bone marrow stromal cells). The *in vivo* relevance of this signature was supported by further bioinformatics analysis, including disease and biological function categories. First, this gene cluster was associated with abnormal morphology of craniofacial structures or craniofacial/neuroectodermal developmental disorders. Secondly, microarray and RT-qPCR analysis and immunostaining showed that genes that encode for key players in the establishment and maintenance of cranial NCC identity such as *SNAI1/2* (Milet and Monsoro-Burq, 2012), *NR2F1/2* (Rada-Iglesias et al., 2012), *ALX3/4* (Beverdam et al., 2001), and *TFAP2A* (Rada-Iglesias et al., 2012; Wang et al., 2011) were all enriched in the NCC population.

Intriguingly, most of the top pathways enriched in this gene cluster were relevant to cholesterol biosynthesis. Although this finding may seem surprising at first glance, it does make sense in the context of potential Hedgehog signaling within the NCC population. Cholesterol modifications are necessary for the production of functional, long-range acting sonic hedgehog (SHH) protein (Ho and Scott, 2002; Lewis et al., 2001) and it is well established that SHH signaling is involved in various craniofacial developmental processes, including survival and proliferation of NCCs (Ahlgren and Bronner-Fraser, 1999; Delloye-Bourgeois et al., 2014; Hu and Helms, 1999). In fact, genes such as *HMGCR*, *HMGCS1*, *DISP1* that are indispensable for cholesterol bio-synthesis or secretion of cholesterol-modified SHH and whose disruption leads to various craniofacial defects (Quintana et al., 2017; Roessler et al., 2009; Schwend and Ahlgren, 2009; Signore et al., 2016) were all part of the NCC gene cluster. These findings raise the enticing possibility that autocrine SHH signaling is involved in maintenance and/or competence of hiPSC-derived NCCs, a hypothesis that will be addressed by future studies.

As far as the second part of our studies is concerned, we used an FBS-rich medium to derive a mesenchymal-like population, NCC-MPCs, from cranial NCCs. NCC-MPCs are characterized by homogeneous expression of known stromal markers such as CD73, CD105, CD90 and CD146, maintain high expression of the nuclear receptor NR2F2 and possess chondrogenic and osteogenic potential. In addition, it is possible to freeze-thaw NCC-MPCs derived from various iPSC lines without obvious phenotypic changes (data not shown). Yet, despite the phenotypic and functional affinities with bone-marrow stromal cells, NCCMPCs and BMSCs were found to be quite distinct in terms of global transcriptome, most probably due to their different developmental origins. This is further supported by the striking differences in the expression pattern of HOX genes between NCC-MPCs and BMSCs, that accurately reflects the HOX code of NCC derivatives *in vivo*, and by the differing degrees of adipogenic competence that is quite high in human BMSCs (Pittenger et al., 1999).

A limitation of our *in vitro* studies is the derivation of NCC-MPCs in FBS-containing culture medium, which, due to its undefined nature, limits the mechanistic understanding of NCC-MPC derivation and maintenance as well as their future clinical applicability. Previous efforts to derive mesenchymal progenitors from iPSCs through an NCC intermediate have addressed this issue by using commercially-available, serum-free media (Fukuta et al., 2014; Hackland et al., 2017). Future studies will investigate the use of specific growth factors, e.g. FGF8 (Shao et al., 2015), or small molecules or both that will allow for the efficient derivation of functional NCC-MPCs from NCCs under serum-free conditions.

On the other hand, NCC-MPCs were shown to have a high degree of similarity, at least by global transcriptional analysis, to dental stem/progenitor cell populations, such as DPSCs, SCAP and PDLSCs that are most likely of neural crest origin (Gronthos et al., 2000; Janebodin et al., 2011; Seo et al., 2004; Sonoyama et al., 2008) and have also multi-lineage differentiation capacity (e.g. DPSCs possess odonto/osteogenic, adipogenic, chondrogenic and neurogenic potential, as reviewed in (Nuti et al., 2016)). Yet, both PCA and clustering analysis of differential gene expression showed that there is a subset of genes whose expression clearly discriminates NCC-MPCs from all dental stem/progenitor cells. RT-qPCR validation of the differential expression of some of the genes showed NCC-MPC-specific expression of *ACKR3* (*CXCR7*), *PTPRB* and *ANKRD1*. The expression of the latter, a canonical YAP/TAZ signaling target, is particularly intriguing, especially given the fact that all cell populations used in our microarray analysis were grown under identical biomechanical conditions. Additionally, *L1CAM* and *MEIS2* were enriched in both NCC-MPCs and NCCs compared to dental stem/progenitor cells. Although we have not been able to reliably detect any putative cell surface marker other than ACKR3 at the protein level, it is likely that a more systematic antibody screen or use of other detection techniques, such as Western blotting, or both are required.

With the exception of *MEIS2*, that is necessary in cranial and heart NCC development (Machon et al., 2015) and osteogenic differentiation of SCAP and DPSCs (Wu et al., 2015), there is little known about potential roles of the other NCC-MPC-specific genes in cranial NCC or dental stem/progenitor cell biology. Future studies will address this issue as well as evaluate the full differentiation repertoire (including dental lineages) of NCC-MPCs or sub-populations thereof. It is also likely that a NCC-MPC counterpart exists *in vivo* and future studies in mouse craniofacial development will investigate this possibility.

4. Materials and methods

4.1. hiPSC culture

hiPSC lines derived from individuals without any known disease, specifically, BU1 (hiPSC clone BU1Cr3–1), BU3 (hiPSC clone BU3–10-Cr2) (Kurmann et al., 2015) and BU7 (hiPSC clone BU7–2-Cr8), were generated from dermal fibroblasts using the hSTEMCCA reprogramming system. These hiPSC lines were obtained from the iPSC bank of the Center for Regenerative Medicine (CReM) of Boston University and Boston Medical Center (http://www.bu.edu/dbin/stemcells/index_iPSC.php). Undifferentiated hiPSCs were maintained on Matrigel (Corning) coated 6-well plates in TeSR-E8 medium (STEMCELL Technologies) with 100 μg/ml Primocin (1:500 dilution, Invivogen) in a 37 °C incubator with 5% CO_2. Approximately every 5–7 days, cells were passaged using Gentle Cell Dissociation Reagent (STEMCELL Technologies) and split into 1:10 ratio.

4.2. NCC differentiation

On Day −1, sufficient volumes of TeSR-E8 (STEMCELL Technologies), DMEM/F12 (Gibco/Invitrogen), and Gentle Cell Dissociation Reagent for passaging were pre-warmed. The well to be passed was washed with 1 ml of Ca^{2+}/Mg^{2+}-free phosphate-buffered saline (PBS). Wash buffer was aspirated and 1 ml of Gentle Cell Dissociation Reagent was added

and the plate was incubated at 37 °C for 8–10 min. Then cells were dislodged by pipetting up and down 1–3 times using a P1000 pipette. The cells were immediately transferred to a tube containing an equal volume of DMEM/F12. The well was washed again with 1 ml of DMEM/F12 to collect any remaining cells. The cells were centrifuged at 300 x *g* for 5 min. Then cells were re-suspended in 1 ml of single-cell passaging medium (TeSR-E8 supplemented with 10 μM Y27632 Rock inhibitor (Sigma) and 100 μg/ml Primocin) and numbers of live cells were counted using a hemocytometer. Cells were plated at 9×10^4 cells per cm^2 density onto Matrigel-coated plates. Cells were incubated at 37 °C and 5% CO_2 for 48 h.

On day 0, differentiation was induced by replacing TeSR-E8 media with NC differentiation media (TeSR-E7 supplemented with 0.5–1 μM CHIR99021 (CHIR), 10 μM SB431542 (R&D Systems) and 100 μg/ml Primocin). Cells were fed every day and passaged every 4–5 days based on their confluency. Starting at day 15, FACS analysis was performed to investigate the expression of NCC markers (HNK1 and p75) by the differentiating cells. Cells were maintained in NCC media (with passing every 4–5 days) until all cultured cells expressed high levels of NCC makers based on FACS analysis, which was usually achieved within 30–40 days depending on the cell line.

4.3. NCC-MPC differentiation

NCCs were disassociated into single cells with TrypLE™ Express reagent (ThermoFisher Scientific), then were plated on non-coated plastic tissue culture dishes with a density of 6.5×10^4 cells/cm^2. NCCs were differentiated using serum-containing media (DMEM/F12 (Gibco) supplemented with 10% FBS (Gibco), 1 mM l-alanyl-l-glutamine, 0.1 mM β-mercaptoethanol (Invitrogen) and 100 μg/ml Primocin), which was changed every other day. Differentiated cells were passaged every 4–5 days using TrypLE™ Express and replated in 1:4 (vol./vol.) ratio. At passage 3, FACS analysis was performed to investigate the expression of MPC (CD73, CD90, CD146, CD13 and CD105), NC (HNK1 and p75), hematopoietic (CD45) and monocyte (CD14) markers. Once the MPC expression profile had been confirmed, cells were either maintained or further differentiated into osteogenic, adipogenic, or chondrogenic lineages.

4.4. Flow cytometry

Differentiating hiPSCs, NCCs, and NCC-MPCs were dissociated using TrypLE™ Express (ThermoFisher Scientific), washed with PBS/2% FBS (PBS+ buffer), and stained for 30 min on ice with monoclonal antibodies (Table S1) and their corresponding isotype controls (BD Biosciences). After staining, cells were washed with 1 ml PBS+, spun down at 300 ×g for 5 min at 4 °C, and cell pellets were either re-suspended in PBS+ if analyzed or in PBS+ with 1× Pen/Strep if sorted. Cells were either analyzed using a FACSCalibur cytometer (BD Biosciences) or sorted using FACSAria III Cell Sorter (BD Biosciences). Data were analyzed using FlowJo software (Tree Star Inc.).

4.5. Tri-lineage differentiation

4.5.1. Osteogenic differentiation—At passage 4–5, NCC-MPCs were detached and dissociated into single cells using pre-warmed TrypLE™ Express and plated into 12-well

culture with a plating density of 10^4 cells/cm^2. Cells were incubated with serum-containing media for 2–4 h, which was then replaced with osteogenic differentiation media (StemPro Osteogenic differentiation kit, Life Technologies) and re-fed every 3–4 days. After 18–23 days, cells were stained using Alizarin Red stain. For Alizarin Red staining, cells were fixed with 4% paraformaldehyde for 30 min, rinsed twice with distilled water, and stained with 2% AR solution (Lifeline Cell Technology) for 2–3 min. Cells were rinsed 3 times with distilled water and visualized under light microscope for image capturing and analysis.

4.5.2. Adipogenic differentiation—At passage 4–5, NCC-MPCs were detached and dissociated into single cells using pre-warmed TrypLE™ Express and plated into 12-well culture with a plating density of 10^5 cells/cm^2. Cells were incubated with serum-containing media for 2–4 h, which was then replaced with adipogenic differentiation media (StemPro adipogenic differentiation kit, Life Technologies) and refed every 3–4 days. After 14 days, cells were stained using the Oil Red O kit (Lifeline Cell Technologies), according to the manufacturer's instructions. Briefly, cells were fixed with 4% paraformaldehyde for 20 min at room temperature, then dehydrated for 5 min using 100% 1,2-Propanediol Dehydration Solution, stained with Oil Red O stain for 30 min at 37 °C, and finally differentially stained using 85% 1,2-Propanediol Stain Differential Solution at room temperature. Cells were rinsed with deionized water and visualized under light microscope for image capturing and analysis.

4.5.3. Chondrogenic differentiation—At passage 4–5, NCC-MPCs were detached and dissociated into single cells using pre-warmed TrypLE™ Express, generating a solution of 1.6×10^6 viable cells/ml. Then 5 μl droplets of cell solution were seeded in 12-well culture plate. Cells were incubated with serum-containing media for 2–4 h, which was then replaced with chondrogenic differentiation media (StemPro chondrogenic differentiation kit, Life Technologies) and refed every 2–3 days. Within 14 days, cells formed micro-masses that were stained using the Alcian Blue staining kit (Lifeline Cell Technologies), according to the manufacturer's instructions. The harvested micro-masses were fixed with 4% PFA for 1 h, then embedded into liquefied Richard-Allan Scientific HistoGel Specimen Processing Gel (ThermoFisher Scientific), solidified on ice for 1 h, and finally paraffin embedded, sectioned, and stained with Alcian Blue stain. The stained micro-masses were visualized under light microscope for image capturing and analysis.

4.6. Quantitative reverse transcriptase polymerase chain reaction (RT-qPCR)

Total RNA extraction was performed the using miRNeasy Mini Kit (Qiagen) and 1 μg DNAse-treated RNA was reverse transcribed using TaqMan Reverse Transcription Reagents (Applied Biosystems). qPCR of complementary DNA (cDNA) was performed in a StepOnePlus Real-Time PCR system (Applied Biosystems) using TaqMan probes (for a complete list of probes see Table S2). Reactions were performed in triplicate. Messenger RNA (mRNA) expression levels were normalized to 18S ribosomal RNA (rRNA) and quantification of relative gene expression, presented as fold change compared to the relevant reference sample, was calculated using the $2^{(-\Delta\Delta CT)}$ method. Biological triplicates from repeat experiments were used to calculate average fold change as well as the standard deviation for each fold change in gene expression, represented by error bars where

indicated. Error bars in graphs represent standard deviations as indicated in the figure legends. Biological sample replicates (N) are also indicated in the legends. Statistically significant differences between conditions (ΔCt values used for RT-qPCR calculations) were determined using two-tailed unpaired Student *t*-tests or as specified in figure legends. Significance is represented as $*p < .05$, $**p < .01$, $***p < .001$, $****p < .0001$.

4.7. Immunostaining

For the TFAP2A staining, NCCs were fixed in 4% paraformaldehyde (Ted Pella, 18,505) for 15 min, and then rinsed twice with PBS. A mouse anti-TFAP2A monoclonal antibody (Developmental Studies Hybridoma Bank, 3B5) was used at a 1:50 dilution and incubation took place overnight at 4 °C. A goat anti-mouse Alexa 547 secondary antibody (ThermoFisher Scientific, A-11003) at 1:200 dilution was added, with incubation for one hour at 37 °C followed by two rinses with PBS. To counterstain nuclei, cultures were incubated for 5 min with 1 μg/ml DAPI (Life Technologies, D1306). Micrographs were acquired using a Nikon Eclipse TS100 and the SPOT Software Version 4.6.1.38.

For the SNAI1, ACTA2 and VIM stainings, NCCs or NCC-MPCs were fixed in 4% paraformaldehyde for 10–15 min, and then rinsed twice with PBS. Cells were permeabilized with 0.1% Triton X-100 for 5 min at room temperature, rinsed with PBS, then blocked using 10% serum for 1 h at room temperature. The following antibodies were used: rabbit anti-SNAI1 (Protein Tech 13,099–1-AP, 1:200 dilution), mouse anti-ACTA2 (Sigma, C6198, Cy3 conjugated, 1:200 dilution), and rabbit anti-VIM (abcam, ab92547, 1:300 dilution) and incubation took place overnight at 4 °C. After three rinses with PBS, a donkey anti-rabbit Alexa 488 (Invitrogen, A21206) (SNAI1 staining) or a donkey anti-rabbit Alexa 546 (Invitrogen, A10040) (VIM staining) at 1:300 dilution was added, with incubation for one hour at room temperature followed by two rinses with PBS. To counterstain nuclei, cultures were incubated for 5 min with 1 μg/ml DAPI (Life Technologies, D1306). Micrographs were captured using a Keyence BZ-X700 fluorescence microscope. Post-acquisition image processing (e.g. black balance) was performed using the BZ-X Analyzer software.

For the NR2F2, MEIS2, and ACKR3 (CXCR7) stainings, NCCs were fixed in 4% paraformaldehyde (Ted Pella, 18505) for 5–10 min, then rinsed twice with PBS. The fixed cells were quenched in 3% H_2O_2 in methanol for 15 min, permeabilized in 0.025% Triton X-100 in PBS for 15 min, and transferred in blocking buffer (4% normal donkey serum in PBS) for 1 h. The following primary antibodies were used alone or in combination (overnight incubation at 4 °C): mouse anti-NR2F2 (1:100 dilution, abcam, ab41859), rabbit anti-MEIS2 (1:50 dilution, Invitrogen, PA5–25432), mouse anti-ACKR3 (1:60 dilution, R&D, MAB42273). Subsequently, the VECTASTAIN® Elite® ABC-HRP Kit (Vector Laboratories; Peroxidase, Rabbit IgG, PK-6101 or Peroxidase, Mouse IgG, PK-6102) in conjunction with the Perkin-Elmer TSA Cyanine 3 System (PerkinElmer, NEL744001KT) was used for fluorescent antigen detection. For dual stains, one of the antigens was detected by incubation with an Alexa 488 anti-mouse or anti-rabbit secondary antibody (1 h incubation, 37 °C). To counterstain nuclei, cultures were incubated for 5 min with 20 μg/ml Hoechst 33342 (1:500 dilution, ThermoFisher Scientific, H3570). Micrographs were captured using a Keyence BZ-X700 fluorescence microscope. Post-acquisition image

processing (e.g. image stitching and black balance) was performed using the BZ-X Analyzer software.

4.8. Microarray analysis

4.8.1. Cell culture and RNA harvesting—RNA was isolated from biological triplicates of NCCs (cultured on Matrigel-coated culture plate with NCC media), NCC-MPCs, dental pulp stem cells (DPSCs), stem cells of the apical papilla (SCAP) and period-ontal ligament stem cells (PDLSCs), and bone marrow mesenchymal stromal cells (BMSCs) (ATCC). Primary human DPSCs, SCAP, and PDLSCs were isolated from freshly extracted teeth (patient details for all primary cells can be found in Table S3). All three primary cell types were maintained in the same dental MSC media (Alpha-modification of Eagle's medium (Gibco/Invitrogen) supplemented with 10% FBS, 1 mM L-glutamine (Gibco/Invitrogen), and 100 μg/ml Primocin). To avoid confounding effects due to different culture media, NCC-MPCs and BMSCs were also maintained in dental MSC media for 2–3 passages before RNA extraction for microarray analysis. Subsequently, cells were harvested and RNA was extracted and submitted to the Boston University Microarray and Sequencing Resource Core Facility. Quality-assessed RNA samples (RIN 9.7–10.0) were used to prepare material for hybridization to Affymetrix Human Gene 2.0 ST arrays based on Affymetrix standard microarray operating procedures.

4.8.2. Microarray data bioinformatics analysis—Human Gene 2.0 ST CEL files were normalized to produce gene-level expression values using the implementation of the Robust Multiarray Average (RMA) (Irizarry et al., 2003) in the affy package (version 1.36.1) (Gautier et al., 2004) included in the Bioconductor software suite (version 2.11) (Gentleman et al., 2004) and an Entrez Gene-specific probeset mapping (17.0.0) from the Molecular and Behavioral Neuroscience Institute (Brainarray, 2017) at the University of Michigan (Dai et al., 2005). Array quality was assessed by computing Relative Log Expression (RLE) and Normalized Unscaled Standard Error (NUSE) using the affyPLM package (version 1.34.0) (Brettschneider et al., 2008). Principal Component Analysis (PCA) was performed using the prcomp R function with expression values that had been normalized across all samples to a mean of zero and a standard deviation of one. Differential expression was assessed using the moderated (empirical Bayesian) ANOVA and *t*-test implemented in the limma package (version 3.14.4) (i.e., creating simple linear models with lmFit, followed by empirical Bayesian adjustment with eBayes). Correction for multiple hypothesis testing was accomplished using the Benjamini-Hochberg false discovery rate (FDR) (Benjamini and Hochberg, 1995). All microarray analyses were performed using the R environment for statistical computing (version 2.15.1). The raw and processed microarray array data have been deposited in the Gene Expression Omnibus (GEO), Series ID GSE113297.

Small-scale heat maps in the figures featuring select gene sets were generated using the online matrix visualization and analysis software Morpheus (https://clue.io/morpheus/).

To perform Ingenuity Pathway Analysis, the set of genes that are strongly expressed in NCCs (482 genes) along with the respective *p* and *q* values were uploaded to the Ingenuity IPA application (Qiagen). 477 genes were mapped and used for subsequent analysis. The

"Canonical Pathways" and the "Diseases & Functions" analytical tools were employed to generate graphs that were then exported as JPEG or TIFF image files.

Supplementary data to this article can be found online at https://doi.org/10.1016/j.scr.2018.10.015.

Supplementary Material

Refer to Web version on PubMed Central for supplementary material.

Acknowledgments

We thank Adam Gower and Eduard Drizik of the Boston University Microarray and Sequencing Resource Core Facility for Affymetrix array processing and bioinformatics support (CTSA grant UL1-TR001430). We are grateful to Brian R. Tilton of the BUSM Flow Cytometry Core for technical assistance, supported by NIH Grant 1UL1TR001430, and Drs. Greg Miller and Marianne James of the CReM, supported by grants R24HL123828 and U01TR001810. We thank Dr. Darrell N. Kotton for helpful comments on the manuscript and Dr. Mina Mina, from UConn Health Center, for insightful discussions. This work was supported in part by grants from the National Institutes of Health (R01 DE019156 to GT-JH). MJ is supported by a Foundation for Endodontics, American Association of Endodontists grant, SLL is supported by a Boston University Clinical and Translational Science Institute training grant (TL1TR001410), and LI is supported by NIH grants R01 HL111574 and R01 HL124280 and an Evans Junior Faculty Research Merit Award.

References

Ahlgren SC, Bronner-Fraser M, 1999. Inhibition of Sonic hedgehog signaling in vivo results in craniofacial neural crest cell death. Curr. Biol 9, 1304–1314. [PubMed: 10574760]

Benjamini Y, Hochberg Y, 1995. Controlling the false discovery rate - a practical and powerful approach to multiple testing. J. R. Stat. Soc. Ser. B-Methodol 57, 289–300.

Beverdam A, Brouwer A, Reijnen M, Korving J, Meijlink F, 2001. Severe nasal clefting and abnormal embryonic apoptosis in Alx3/Alx4 double mutant mice. Development 128, 3975–3986. [PubMed: 11641221]

Brainarray, 2017. Description of Customized CDF Files Retrieved October 20 2017, from. http://brainarray.mbni.med.umich.edu/Brainarray/Database/CustomCDF.

Brettschneider J, Collin F, Bolstad BM, Speed TP, 2008. Quality assessment for short oligonucleotide microarray data. Technometrics 50, 241–264.

Chai Y, Jiang XB, Ito Y, Bringas P, Han J, Rowitch DH, Soriano P, McMahon AP, Sucov HM, 2000. Fate of the mammalian cranial neural crest during tooth and mandibular morphogenesis. Development 127, 1671–1679. [PubMed: 10725243]

Chambers SM, Fasano CA, Papapetrou EP, Tomishima M, Sadelain M, Studer L, 2009. Highly efficient neural conversion of human ES and iPS cells by dual inhibition of SMAD signaling. Nat. Biotechnol 27, 275–280. [PubMed: 19252484]

Creuzet S, Couly G, Vincent C, Le Douarin NM, 2002. Negative effect of Hox gene expression on the development of the neural crest-derived facial skeleton. Development 129, 4301–4313. [PubMed: 12183382]

Dai MH, Wang PL, Boyd AD, Kostov G, Athey B, Jones EG, Bunney WE, Myers RM, Speed TP, Akil H, Watson SJ, Meng F, 2005. Evolving gene/transcript definitions significantly alter the interpretation of GeneChip data. Nucleic Acids Res 33, 9.

de Croze N, Maczkowiak F, Monsoro-Burq AH, 2011. Reiterative AP2a activity controls sequential steps in the neural crest gene regulatory network. Proc. Natl. Acad. Sci. U. S. A 108, 155–160. [PubMed: 21169220]

Delloye-Bourgeois C, Rama N, Brito J, Le Douarin N, Mehlen P, 2014. Sonic Hedgehog promotes the survival of neural crest cells by limiting apoptosis induced by the dependence receptor CDON during branchial arch development. Biochem. Biophys. Res. Commun 452, 655–660. [PubMed: 25193697]

Dominici M, Le Blanc K, Mueller I, Slaper-Cortenbach I, Marini FC, Krause DS, Deans RJ, Keating A, Prockop DJ, Horwitz EM, 2006. Minimal criteria for defining multipotent mesenchymal stromal cells. The international society for cellular therapy position statement. Cytotherapy 8, 315–317. [PubMed: 16923606]

Dupin E, Le Douarin NM, 2014. The neural crest- a multifaceted structure of the vertebrates. Birth Defects Res. C Embryo Today Rev 102, 187–209.

Fukuta M, Nakai Y, Kirino K, Nakagawa M, Sekiguchi K, Nagata S, Matsumoto Y, Yamamoto T, Umeda K, Heike T, Okumura N, Koizumi N, Sato T, Nakahata T, Saito M, Otsuka T, Kinoshita S, Ueno M, Ikeya M, Toguchida J, 2014. Derivation of mesenchymal stromal cells from pluripotent stem cells through a neural crest lineage using small molecule compounds with defined media. PLoS One 9, 25.

Gautier L, Cope L, Bolstad BM, Irizarry RA, 2004. affy - analysis of Affymetrix GeneChip data at the probe level. Bioinformatics 20, 307–315. [PubMed: 14960456]

Gentleman RC, Carey VJ, Bates DM, Bolstad B, Dettling M, Dudoit S, Ellis B, Gautier L, Ge YC, Gentry J, Hornik K, Hothorn T, Huber W, Iacus S, Irizarry R, Leisch F, Li C, Maechler M, Rossini AJ, Sawitzki G, Smith C, Smyth G, Tierney L, Yang JYH, Zhang JH, 2004. Bioconductor: open software development for computational biology and bioinformatics. Genome Biol 5, 16.

Gronthos S, Mankani M, Brahim J, Robey PG, Shi S, 2000. Postnatal human dental pulp stem cells (DPSCs) in vitro and in vivo. Proc. Natl. Acad. Sci. U. S. A 97, 13625–13630. [PubMed: 11087820]

Hackland JOS, Frith TJR, Thompson O, Navarro AM, Garcia-Castro MI, Unger C, Andrews PW, 2017. Top-down inhibition of BMP signaling enables robust induction of hPSCs into neural crest in fully defined, xeno-free conditions. Stem Cell Rep 9, 1043–1052.

Ho KS, Scott MP, 2002. Sonic hedgehog in the nervous system: functions, modifications and mechanisms. Curr. Opin. Neurobiol 12, 57–63. [PubMed: 11861165]

Hu D, Helms JA, 1999. The role of Sonic hedgehog in normal and abnormal cranio-facial morphogenesis. Development 126, 4873–4884. [PubMed: 10518503]

Huang M, Miller ML, McHenry LK, Zheng TN, Zhen QQ, Ilkhanizadeh S, Conklin BR, Bronner ME, Weiss WA, 2016. Generating trunk neural crest from human pluripotent stem cells. Sci. Rep 6, 9. [PubMed: 28442706]

Irizarry RA, Hobbs B, Collin F, Beazer-Barclay YD, Antonellis KJ, Scherf U, Speed TP, 2003. Exploration, normalization, and summaries of high density oligonucleotide array probe level data. Biostatistics 4, 249–264. [PubMed: 12925520]

Janebodin K, Horst OV, Ieronimakis N, Balasundaram G, Reesukumal K, Pratumvinit B, Reyes M, 2011. Isolation and characterization of neural crest-derived stem cells from dental pulp of neonatal mice. PLoS One 6.

Jiang XH, Gwye Y, McKeown SJ, Bronner-Fraser M, Lutzko C, Lawlor ER, 2009. Isolation and characterization of neural crest stem cells derived from in vitro-differentiated human embryonic stem cells. Stem Cells Dev 18, 1059–1070. [PubMed: 19099373]

Kurmann AA, Serra M, Hawkins F, Rankin SA, Mori M, Astapova I, Ullas S, Lin S, Bilodeau M, Rossant J, Jean JC, Ikonomou L, Deterding RR, Shannon JM, Zorn AM, Hollenberg AN, Kotton DN, 2015. Regeneration of thyroid function by transplantation of differentiated pluripotent stem cells. Cell Stem Cell 17, 527–542. [PubMed: 26593959]

Lee G, Papapetrou EP, Kim H, Chambers SM, Tomishima MJ, Fasano CA, Ganat YM, Menon J, Shimizu F, Viale A, Tabar V, Sadelain M, Studer L, 2009. Modelling pathogenesis and treatment of familial dysautonomia using patient-specific iPSCs. Nature 461, 402–U100. [PubMed: 19693009]

Leucht P, Kim JB, Amasha R, James AW, Girod S, Helms JA, 2008. Embryonic origin and Hox status determine progenitor cell fate during adult bone regeneration. Development 135, 2845–2854. [PubMed: 18653558]

Lewis PM, Dunn MP, McMahon JA, Logan M, Martin JF, St-Jacques B, McMahon AP, 2001. Cholesterol modification of sonic hedgehog is required for long-range signaling activity and effective modulation of signaling by Ptc1. Cell 105, 599–612. [PubMed: 11389830]

Machon O, Masek J, Machonova O, Krauss S, Kozmik Z, 2015. Meis2 is essential for cranial and cardiac neural crest development. BMC Dev. Biol 15, 16. [PubMed: 25888082]

Menendez L, Yatskievych TA, Antin PB, Dalton S, 2011. Wnt signaling and a Smad pathway blockade direct the differentiation of human pluripotent stem cells to multipotent neural crest cells. Proc. Natl. Acad. Sci. U. S. A 108, 19240–19245. [PubMed: 22084120]

Menendez L, Kulik MJ, Page AT, Park SS, Lauderdale JD, Cunningham ML, Dalton S, 2013. Directed differentiation of human pluripotent cells to neural crest stem cells. Nat. Protoc 8, 203–212. [PubMed: 23288320]

Mica Y, Lee G, Chambers SM, Tomishima MJ, Studer L, 2013. Modeling neural crest induction, melanocyte specification, and disease-related pigmentation defects in hESCs and patient-specific iPSCs. Cell Rep 3, 1140–1152. [PubMed: 23583175]

Milet C, Monsoro-Burq AH, 2012. Neural crest induction at the neural plate border in vertebrates. Dev. Biol 366, 22–33. [PubMed: 22305800]

Mumme M, Barbero A, Miot S, Wixmerten A, Feliciano S, Wolf F, Asnaghi AM, Baumhoer D, Bieri O, Kretzschmar M, Pagenstert G, Haug M, Schaefer DJ, Martin I, Jakob M, 2016. Nasal chondrocyte-based engineered autologous cartilage tissue for repair of articular cartilage defects: an observational first-in-human trial. Lancet 388, 1985–1994. [PubMed: 27789021]

Nuti N, Corallo C, Chan BMF, Ferrari M, Gerami-Naini B, 2016. Multipotent differentiation of human dental pulp stem cells: a literature review. Stem Cell Rev. Rep 12, 511–523. [PubMed: 27240827]

Osafune K, Caron L, Borowiak M, Martinez RJ, Fitz-Gerald CS, Sato Y, Cowan CA, Chien KR, Melton DA, 2008. Marked differences in differentiation propensity among human embryonic stem cell lines. Nat. Biotechnol 26, 313–315. [PubMed: 18278034]

Pittenger MF, Mackay AM, Beck SC, Jaiswal RK, Douglas R, Mosca JD, Moorman MA, Simonetti DW, Craig S, Marshak DR, 1999. Multilineage potential of adult human mesenchymal stem cells. Science (New York, N.Y.) 284, 143–147.

Quintana AM, Hernandez JA, Gonzalez CG, 2017. Functional analysis of the zebrafish ortholog of HMGCS1 reveals independent functions for cholesterol and isoprenoids in craniofacial development. PLoS One 12, 17.

Rada-Iglesias A, Bajpai R, Prescott S, Brugmann SA, Swigut T, Wysocka J, 2012. Epigenomic annotation of enhancers predicts transcriptional regulators of human neural crest. Cell Stem Cell 11, 633–648. [PubMed: 22981823]

Rada-Iglesias A, Prescott SL, Wysocka J, 2013. Human genetic variation within neural crest enhancers: molecular and phenotypic implications. Philos. Trans. R. Soc. B Biol. Sci 368, 8.

Ring DB, Johnson KW, Henriksen EJ, Nuss JM, Goff D, Kinnick TR, Ma ST, Reeder JW, Samuels I, Slabiak T, Wagman AS, Hammond MEW, Harrison SD, 2003. Selective glycogen synthase kinase 3 inhibitors potentiate insulin activation of glucose transport and utilization in vitro and in vivo. Diabetes 52, 588–595. [PubMed: 12606497]

Roessler E, Ma Y, Ouspenskaia MV, Lacbawan F, Bendavid C, Dubourg C, Beachy PA, Muenke M, 2009. Truncating loss-of-function mutations of DISP1 contribute to holoprosencephaly-like microform features in humans. Hum. Genet 125, 393–400. [PubMed: 19184110]

Schwend T, Ahlgren SC, 2009. Zebrafish con/disp1 reveals multiple spatiotemporal requirements for Hedgehog-signaling in craniofacial development. BMC Dev. Biol 9, 22. [PubMed: 19291313]

Seo BM, Miura M, Gronthos S, Mark Bartold P, Batouli S, Brahim J, Young M, Gehron Robey P, Wang CY, Shi S, 2004. Investigation of multipotent postnatal stem cells from human periodontal ligament. Lancet 364, 149–155. [PubMed: 15246727]

Shao MY, Liu C, Song YN, Ye WD, He W, Yuan GH, Gu SP, Lin CX, Ma L, Zhang YD, Tian WD, Hu T, Chen YP, 2015. FGF8 signaling sustains progenitor status and multipotency of cranial neural crest-derived mesenchymal cells in vivo and in vitro. J. Mol. Cell Biol 7, 441–454.

Sharpe PT, 2016. Dental mesenchymal stem cells. Development 143, 2273–2280. [PubMed: 27381225]

Signore IA, Jerez C, Figueroa D, Suazo J, Marcelain K, Cerda O, Flores AC, 2016. Inhibition of the 3-hydroxy-3-methyl-glutaryl-CoA reductase induces orofacial defects in zebrafish. Birth Defects Res. Part A Clin. Mol. Teratol 106, 814–830.

Simoes-Costa M, Bronner ME, 2015. Establishing neural crest identity: a gene regulatory recipe. Development 142, 242–257. [PubMed: 25564621]

Simoes-Costa M, Tan-Cabugao J, Antoshechkin I, Sauka-Spengler T, Bronner ME, 2014. Transcriptome analysis reveals novel players in the cranial neural crest gene regulatory network. Genome Res 24, 281–290. [PubMed: 24389048]

Sonoyama W, Liu Y, Yamaza T, Tuan RS, Wang S, Shi S, Huang GTJ, 2008. Characterization of the apical papilla and its residing stem cells from human immature permanent teeth: A pilot study. J. Endod 34, 166–171. [PubMed: 18215674]

Wang WD, Melville DB, Montero-Balaguer M, Hatzopoulos AK, Knapik EW, 2011. Tfap2a and Foxd3 regulate early steps in the development of the neural crest progenitor population. Dev. Biol 360, 173–185. [PubMed: 21963426]

Wu ZF, Wang JS, Dong R, Wang LP, Fan ZP, Liu DY, Wang SL, 2015. Depletion of MEIS2 inhibits osteogenic differentiation potential of human dental stem cells. Int. J. Clin. Exp. Med 8, 7220–7230. [PubMed: 26221261]

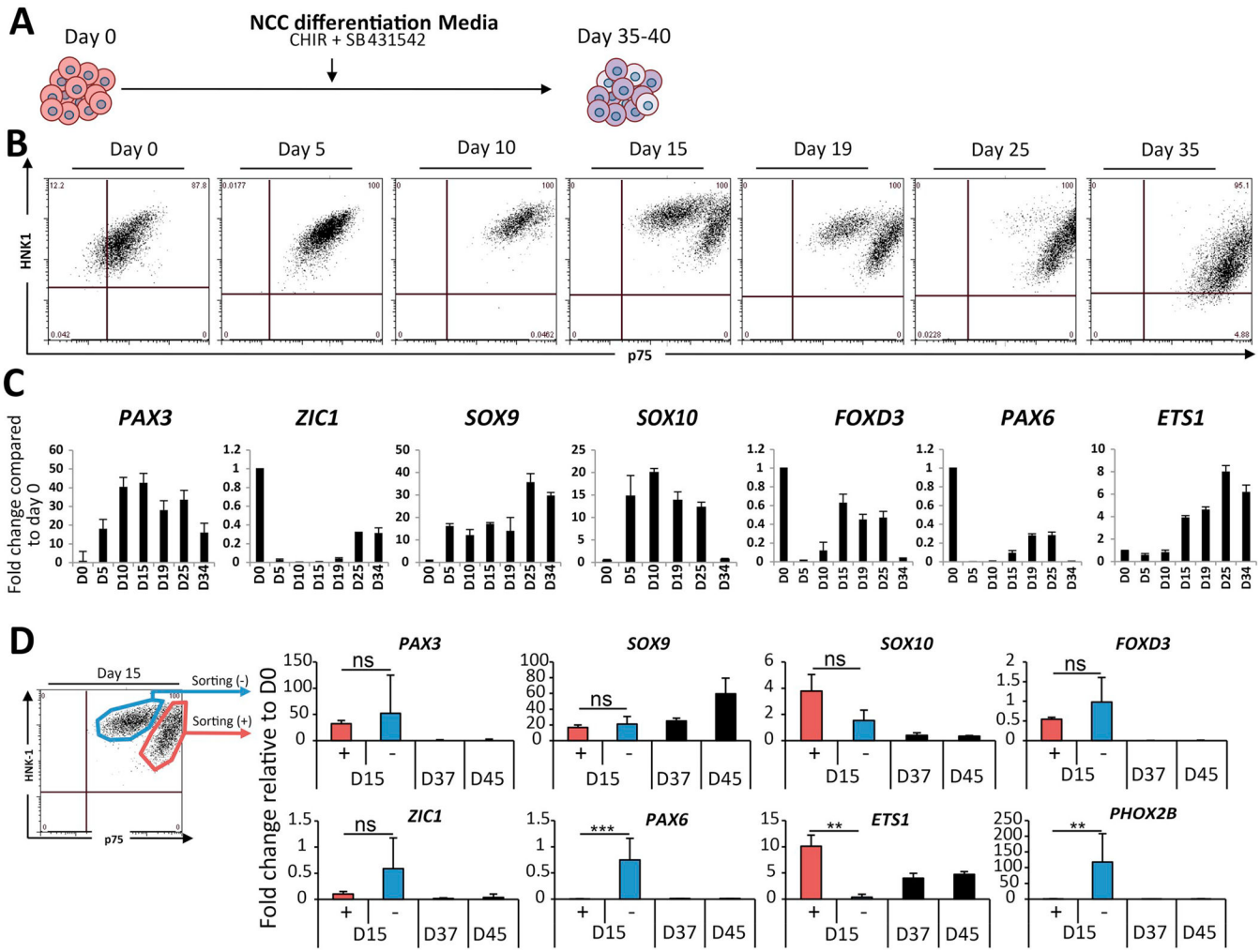

Fig. 1.

Derivation and characterization of putative NCCs from BU3 hiPSCs.

(A) Differentiation protocol for the derivation of putative NCCs from hiPSCs showing the added factors and the duration of the differentiation.

(B) Bivariate flow cytometry dot plots demonstrating the temporal expression patterns of HNK1 and p75 in the course of NCC differentiation (D0-D35).

(C) Kinetics of NCC and neuronal marker expression by RT-qPCR. Fold changes are calculated relative to D0 undifferentiated hiPSCs. Error bars represent standard deviation ($N = 3$).

(D) Schematic showing the sorting of two populations p75(+) ($p75^{bright}$) and p75(−) ($p75^{dim}$) on D15 of NCC differentiation (left panel). Transcriptional analysis by RT-qPCR of NCC- and neuronal-related genes of the sorted populations on D15 as well as of $p75^{bright}$ populations on D37 and D45. Error bars represent standard deviation (N = 3).

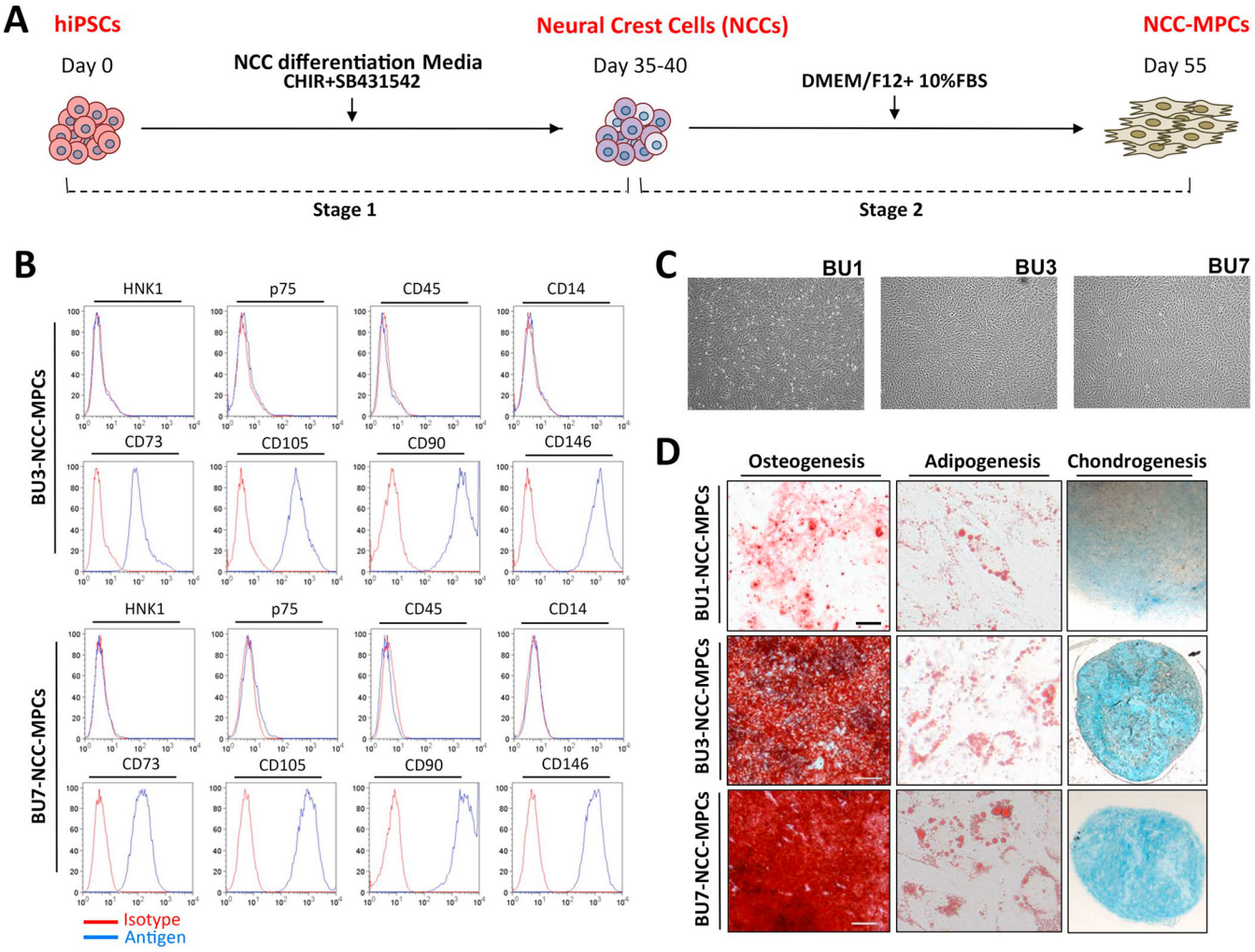

Fig. 2.

Derivation of NCC-MPCs from hiPSCs through a cranial NCC intermediate.

(A) Differentiation protocol showing the multi-step derivation of NCC-MPCs from hiPSCs.

(B) Flow cytometry histograms depicting the expression levels of various neural crest, stromal and hematopoietic cell surface markers in NCC-MPCs after three passages. Data are shown for two hiPSC lines (BU3 and BU7). The red line indicates staining with an isotype control for each antibody.

(C) Phase contrast micrographs of near confluent NCC-MPCs derived from three hiPSC lines.

(D) Brightfield micrographs of NCC-MPCs derived from three hiPSC lines following incubation in osteogenic, adipogenic and chondrogenic media. Calcium deposition indicating osteogenic differentiation was detected by Alizarin Red staining (left panel), oil droplets indicating adipogenic differentiation were detected by Oil Red O staining (middle panel) and glucosaminoglycans indicating chondrogenic differentiation were detected by Alcian Blue staining (right panel).

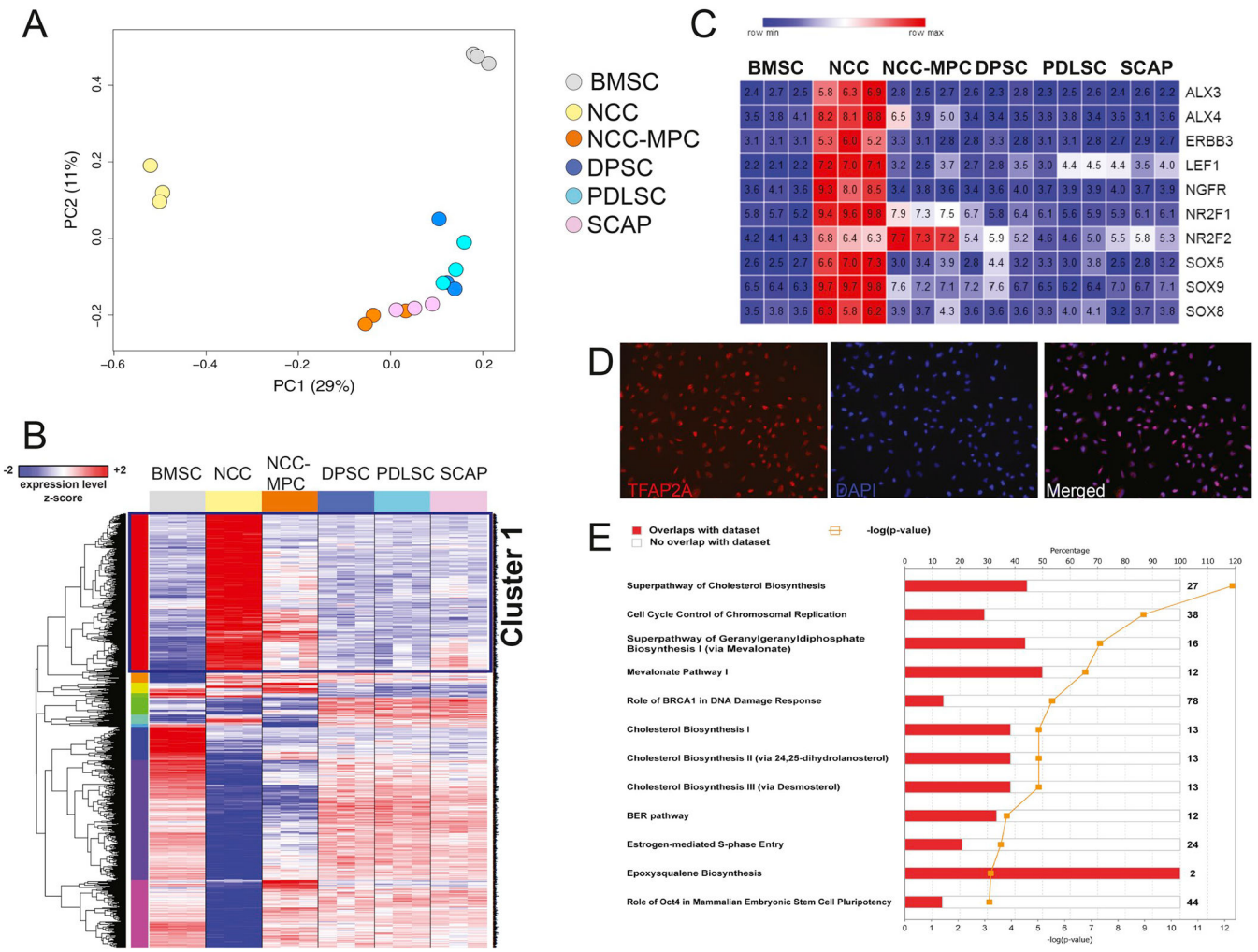

Fig. 3.

Genome-wide transcriptomic analysis of hiPSC-derived NCCs and NCC-MPCs.

(A) Principal component analysis (PCA) plot of microarray populations (NCCs, NCC-MPCs and dental stem/progenitor cell populations). The x and y axes depict the PC1 and PC2, respectively.

(B)Microarray heat map: the heat map shows the top differentially expressed genes (1327 genes, FDR < 10^{-6}, |fold change| > 4) across all groups (NCCs, NCCMPCs, DPSCs, PDLSCs, SCAP and BMSCs) clustered by samples in triplicate (columns) and expression clusters (rows). Cluster 1 that differentiates NCCs from all other populations is indicated on the right. The log2 (expression) values for each gene were z-score-normalized to a mean of zero and standard deviation of 1 across all samples in each row; blue and red indicate z-scores less than −2 or > 2, respectively, and white indicates a z-score of 0 (row-wise mean).

(C) Heat map showing differential gene expression of select NCC-related genes across the same groups as in (B).

(D) Fluorescence micrographs of NCC culture (BU1 hiPSC line) stained for TFAP2A.

(E) Top pathways of the Cluster 1 genes derived from Ingenuity Pathway Analysis. Cutoff p-value = 10^{-3}.

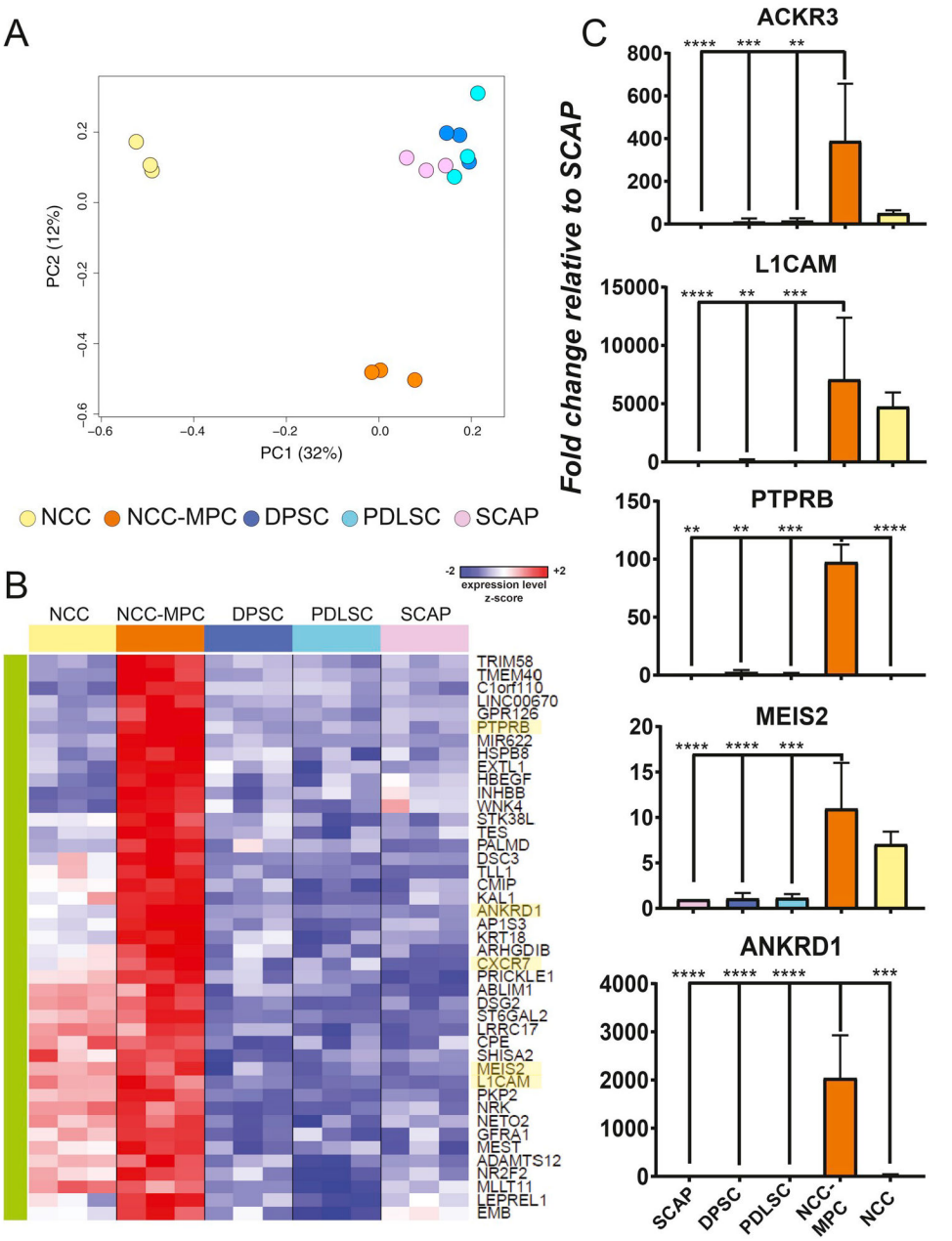

Fig. 4.

Transcriptional signature of NCC-MPCs.

(A) PCA plot of all populations without BMSCs. The x and y axes depict the PC1 and PC2, respectively.

(B) Enlarged view of Cluster 3 of the heat map in Fig. S4C. This cluster contains 43 genes (FDR < 10^{-6}, |fold change| > 4). The log2 (expression) values for each gene were z-score-normalized to a mean of zero and standard deviation of 1 across all samples in each row; blue and red indicate z-scores less than −2 or > 2, respectively, and white indicates a z-score of 0 (row-wise mean).

(C) RT-qPCR validation of five genes contained in (B). Fold changes are calculated relative to SCAP. Error bars represent standard deviation (N = 3). **: $p < .01$, ***: $p < .001$, ****: $p < .0001$.

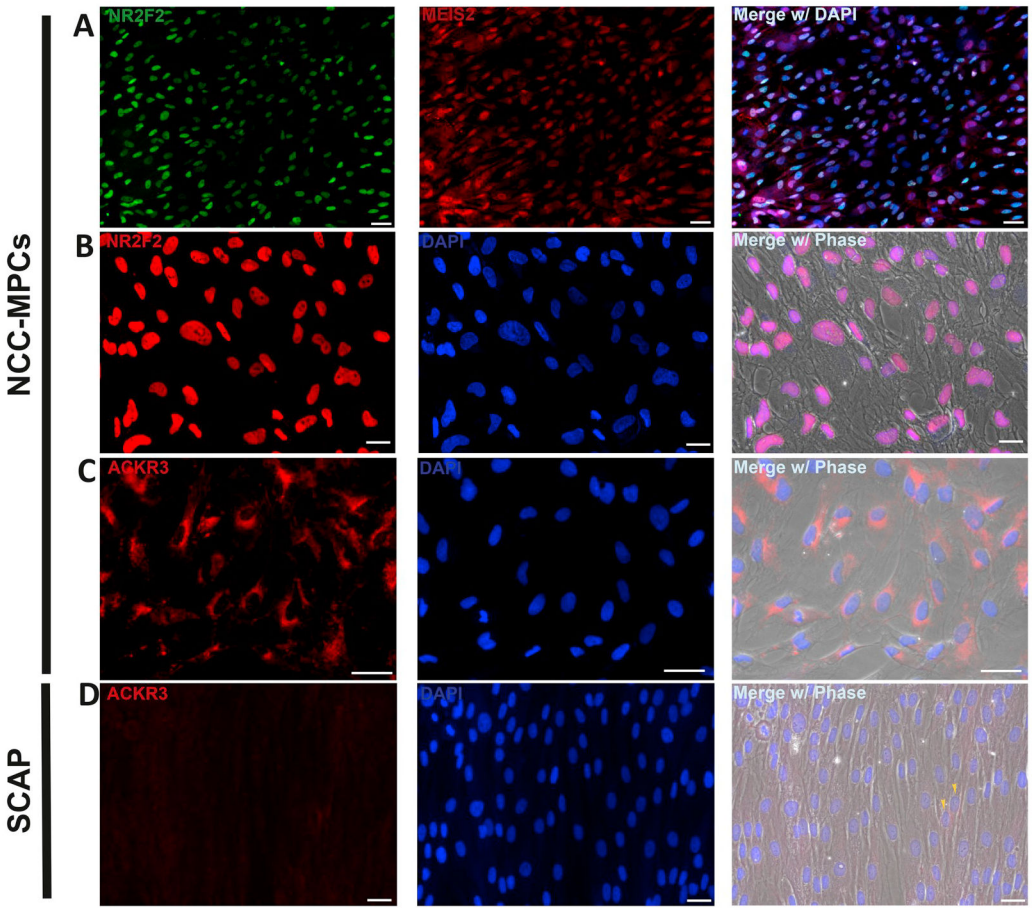

Fig. 5.

NCC-MPCs co-express ACKR3, MEIS2 and NR2F2.

Representative fluorescent micro-graphs of NCC-MPCs stained for (A) NR2F2 and MEIS2 (B) NR2F2, and (C) ACKR3 (CXCR7) and of SCAP stained for (D) ACKR3 (CXCR7). Arrowheads indicate two cells with low ACKR3 expression. Scale bar, 50 μm for (A), (C) and (D), 30 μm for (B).